DOI 10.1007/s10812-025-01842-z
Journal of Applied Spectroscopy, Vol. 91, No. 6, January, 2025 (Russian Original Vol. 91, No. 6, November–December, 2024)

EFFECT OF THE OXIDATIVE ANNEALING TEMPERATURE ON THE STRUCTURAL AND OPTICAL CHARACTERISTICS OF TIN OXIDE FILMS

V. K. Ksenevich,[a,b,*] V. A. Dorosinets,[a] M. A. Samarina,[a] D. V. Adamchuk,[c] G. Abdurakhmanov,[d] and H. Liu[b,e]

UDC 535.375.5:546.811/.814

Results are given for a study of the crystal structure and optical characteristics of disordered tin oxide films. The synthesis of these films was carried out by means of magnetron sputtering of a tin target on a glass substrate followed by two-stage annealing in the air. The microstructure of the tin oxide films was analyzed by x-ray diffraction and Raman spectroscopy. Transmission spectra of the samples were taken in the wavelength range λ = 200–3000 nm. The optical constants of the thin tin oxide films, namely, the refractive index n and absorption coefficient α, relative to wavelength were determined using the envelope method. Feasibility was shown for the preparation of tin oxide films with control of the optical parameters (absorption coefficient α up to 82% in the visible range of the electromagnetic spectrum, refractive index n in the range 2–2.6, and Tauc optical gap in the range 2.62–3.46 eV) by adjusting the temperature in the second stage of the oxidative annealing process in the range 325–475°C.

Keywords: *tin oxide films, magnetron sputtering, oxidative annealing, x-ray diffraction, Raman spectroscopy, absorption coefficient.*

Introduction. Tin dioxide (SnO_2) is a wide-gap *n*-type semiconductor with band gap E_g = 3.6 eV at 300 K, which imparts high optical transparency in the visible spectrum to unalloyed SnO_2. Alloying SnO_2 with donor additives such as antimony or fluorine, which form fine band gap structure, permits us to obtain materials transparent in the visible and UV regions with high electrical conductance. The optimal ratio of transmission and conductance coefficients for SnO_2, as in the case of other wide band metal oxide semiconductors such as ZnO and In_2O_3, is also achieved by the introduction of a high concentration of intrinsic defects during the preparation process, which leads to a nonstoichiometric composition of the material. Thus, the high electrical conductance of unalloyed tin dioxide is usually related to the presence of oxygen vacancies, forming fine donor level structure in the band gap and providing for good electronic conductance [1–3]. The electrical conductance of SnO_2 with a large amount the intrinsic defects can vary in a wide range up to metallic conductance when there is a high concentration of oxygen vacancies [4, 5]. Indium oxide semiconductors are currently most commonly used in optoelectronic devices. However, due to the limited proven reserves of indium, SnO_2 films are finding increasing use in functional optoelectronic elements. For example, SnO_2 films can be used as conducting coatings in sensor panels [6], transparent conducting electrodes for solar cells [7, 8], resistive gas sensors [9, 10], UV light sensors [11], as well as in lithium-ion [12] and sodium-ion batteries [13]. We should note that nonstoichiometric SnO_2 has a number of significant advantages such as low cost, nontoxicity, and rather high mechanical strength.

Since tin can have two oxidation levels in its oxides (+2 and +4), two stable oxide phases are possible, namely, tin(II) monoxide (SnO) and tin(IV) dioxide (SnO_2). In contrast to direct bandgap tin dioxide, tin monoxide is an indirect bandgap semiconductor with a wide band gap E_g = 2.5 eV at 300 K and *p*-type conductance due to the presence of tin vacancies [6]. Multiphase samples containing the SnO phase in addition to SnO_2 as well as nonstoichiometric Sn_2O_3 and Sn_3O_4 phases

*To whom correspondence should be addressed.

[a]Belarusian State University, Minsk, Belarus; email: Ksenevich@bsu.by; [b]Dalian University of Technology and Belarusian State University Joint Institute & Innovation Center, Dalian, China; [c]Institute for Nuclear Problems, Belarusian State University, Minsk, Belarus; [d]National University of Uzbekistan, Tashkent, Uzbekistan; [e]Key Laboratory of Materials Modification by Laser, Ion and Electron Beams, Dalian University of Technology, Ministry of Education, Dalian, China.
Translated from Zhurnal Prikladnoi Spektroskopii, Vol. 91, No. 6, pp. 813–820, November–December, 2024. Original article submitted June 4, 2024.

can be obtained by varying aspects of the tin oxide film preparation procedure. In particular, the crystal structure and phase composition of tin oxide films, when prepared by reactive magnetron sputtering with subsequent annealing in the air, can be varied by changing the amount of oxygen in the argon-oxygen plasma during the sputtering and the temperature of the subsequent oxidative annealing [14–17].

Multiphase character of tin oxide films can be advantageous for the creation of thermoelectric materials containing such films due to decreased thermal conductance attributed to disorder in the structure. Vieira et al. [18] have shown the possibility of creating thermoelectric sensor panels using SnO_x containing both SnO and SnO_2 phases. Multiphase structures with tin oxides can also be used for creating gas sensors. Shanmugasundaram et al. [19] have found enhanced sensitivity to oxygen in comparison with samples with monophase SnO_2 attributed to the *p–n* transitions in SnO/SnO_2 nanocomposites. Greater sensitivity to NO_2 and decreased working temperature were also found for SnO/SnO_2 and SnO/Sn_3O_4 nanocomposites [20, 21].

The significant change in the conductance in going from nonstoichiometric SnO_2 films to multiphase tin oxide films can also involve change in the optical properties of this oxide such as band gap width, absorption coefficient, and refraction index, which permits us to obtain tin oxide films with electrical and optical characteristics required for specific applications by adjusting the preparation conditions.

In the present work, we studied the structural and optical properties of thin tin oxide films prepared on glass substrates by means of direct current magnetron sputtering with subsequent oxidative annealing in the air. A study was carried out on the effect of the annealing temperature on the phase composition of these films and their optical properties such as absorption coefficient, refraction index, and optical absorption edge.

Experimental. Thin tin oxide films were synthesized by magnetron sputtering of a 99.99%-pure tin target with subsequent two-stage oxidative annealing in the air at 200°C for 2 h in the first stage and at different temperatures in the range 325–475°C for 1 h in the second stage. The microstructure of the tin oxide films was analyzed by x-ray diffraction and Raman spectroscopy. The x-ray structural analysis of the films was carried out using a Rigaku Ultima IV x-ray diffractometer in parallel beam configuration and monochromatic CuK_α radiation (0.15406 nm) with a D/teX high-speed x-ray detector. The Raman spectra were taken at room temperature using a backscattering Lotis TII Nanofinder High End spectral analysis complex. The spectrometer resolution was 0.3 cm^{-1}. The exciting beam diameter was ~1 μm upon applying 0.6 mW power to the sample, The exciting radiation of a solid laser with wavelength 532 nm was used. The optical transmission spectra of the samples were taken using a Photon RT spectrophotometer in the range 200–3000 nm. The spectral resolution of the instrument was 1.2 nm.

Results and Discussion. The x-ray diffractograms of the samples are shown in Fig. 1. Analysis of these diffractograms suggests that our synthesis method yields polycrystalline multiphase tin oxide films containing both tetragonal SnO and tetragonal SnO_2 with rutile structure as well as nonstoichiometric Sn_2O_3 and Sn_3O_4 phases [22–25]. Variation of the temperature in the second annealing stage in the range 325–475°C after prior annealing for 2 h at 200°C permits us to obtain different phase compositions of the resultant samples. Thus, the diffractogram of the film annealed at 325°C in the second annealing stage shows x-ray reflections near 29.9°, 33.3°, and 57.4° from the (101), (110), and (211) SnO planes, respectively. In this case, reflections typical of SnO_2 phase do not virtually manifest themselves for this sample. The formation of the SnO_2 phase becomes obvious for the film annealed at 400°C. In particular, on the diffractogram of this sample reflections can be observed near 26.6°, 33.9°, and 52.2° that can be caused by reflection of x-ray radiation from the (110), (101), and (211) SnO_2 phase, respectively. Greater intensity of peaks characteristic of the SnO and SnO_2 phases is observed upon further increasing the temperature in the second annealing stage, which indicates more perfect crystal structure in the prepared films. We should note that, in addition to reflections characteristic of SnO and SnO_2, the diffractograms of the films show peaks due to reflection from the (011) and (0–21) planes of the nonstoichiometric Sn_2O_3 phase near 26.9° and 31.6°, respectively, and from the Sn_3O_4 phase near 38.2°.

The effect of the second oxidative annealing stage on the structural properties and phase composition of these tin oxide films is also seen in their Raman spectra (Fig. 2a). The spectra of the films annealed at 325°C show pronounced lines near 110 and 211 cm^{-1} corresponding to the E_g and A_{1g} vibrational modes of the SnO phase [26] as well as a line near 78 cm^{-1} corresponding to the Sn_2O_3 phase [27]. Furthermore, the Raman spectrum of this sample shows weak lines near 315, 695, and 750 cm^{-1} corresponding to the SnO_2 phase [28]. These findings indicate that the SnO phase is predominantly formed after annealing at 325°C. When the temperature in the second annealing stage is raised to 350°C, the intensities of the Raman peaks corresponding to the SnO phase are diminished and the intensity of the peaks corresponding to the SnO_2 phase and nonstoichiometric Sn_2O_3 or Sn_3O_4 phases are enhanced. In particular, the line near 211 cm^{-1} characteristic of the

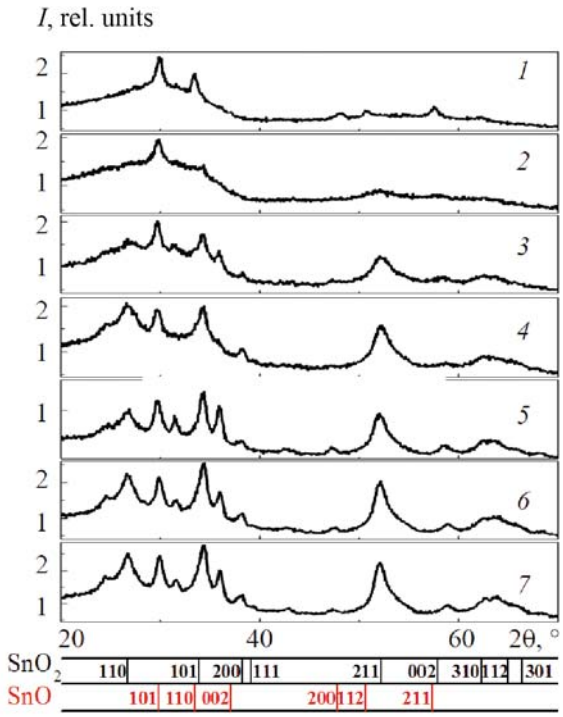

Fig. 1. X-ray diffractograms of tin oxide films obtained by magnetron sputtering of a tin target with subsequent annealing in the air at 200°C for 2 h in the first stage and 325 (1), 350 (2), 375 (3), 400 (4), 425 (5), 450 (6), and 475°C (7) for 1 h in the second stage.

SnO phase is not seen for films annealed at ≥350°C but we find lines near 125, 140, and 250 cm^{-1} corresponding to vibrations characteristic for the SnO_2, Sn_3O_4, and Sn_2O_3 phases [29]. A further increase in the annealing temperature to 425°C leads to improved crystallinity of the films and enhancement of the intensity of the peaks corresponding to the SnO_2 phase. The Raman spectra of the films annealed in the second stage at 450 and 475°C showed a decrease in the intensity of the lines corresponding to vibrational modes of both SnO and SnO_2. The decrease in the intensity of the lines characteristic of SnO and the nonstoichiometric phases is attributed to increased content of the SnO_2 phase in these films. The lower intensity of the lines characteristic for SnO_2 in the spectra of the films annealed at 450° and 475°C relative to the samples annealed in the range 350–425°C can be a Raman resonance effect. The essence of this effect lies in the enhanced intensity of inelastic light scattering when the energy of the laser radiation excitation is the same as the energy of the electronic transitions in the material studied [29]. The Raman spectra were taken using exciting laser radiation with $\lambda = 532$ nm, which corresponds to 2.33 eV. The band gap width for SnO E_g = 2.5–3.0 eV, which is much lower than E_g = 3.6 eV for SnO_2 [6]. Thus, an increase in the SnO_2 content in the tin oxide multiphase films should lead to an increase in the Tauc optical gap. The x-ray diffraction analysis data and the Raman spectral results showed that this occurs with an increase in the temperature of the second annealing stage. Thus, the excitation energy becomes much less than the energy of possible electronic transitions in the films annealed at 450 and 475°C, leading to reduced probability of Raman resonance and, correspondingly, decreased intensity of the Raman lines.

The transmission spectra of the samples in the range 200–3000 nm were taken to evaluate the Tauc optical gap of the tin oxide films prepared on glass substrates at different temperatures in the second annealing stage in the air. Oscillatory nature is found for the transmission spectra shown in Fig. 2b due to interference effects in the film–substrate system. The prepared thin films have a high transmission coefficient in the range λ = 350–3000 nm.

The optical characteristics of the thin tin oxide films such as the refraction index $n(\lambda)$ and absorption coefficient $\alpha(\lambda)$ as well as the film thickness d were determined from the interference-type transmission spectra using the envelope method [30] employed in the case of the weak light absorption by the thin film and high transparency of the substrate whose thickness is much greater than the film thickness. The essence of this method lies in the following. The transmission

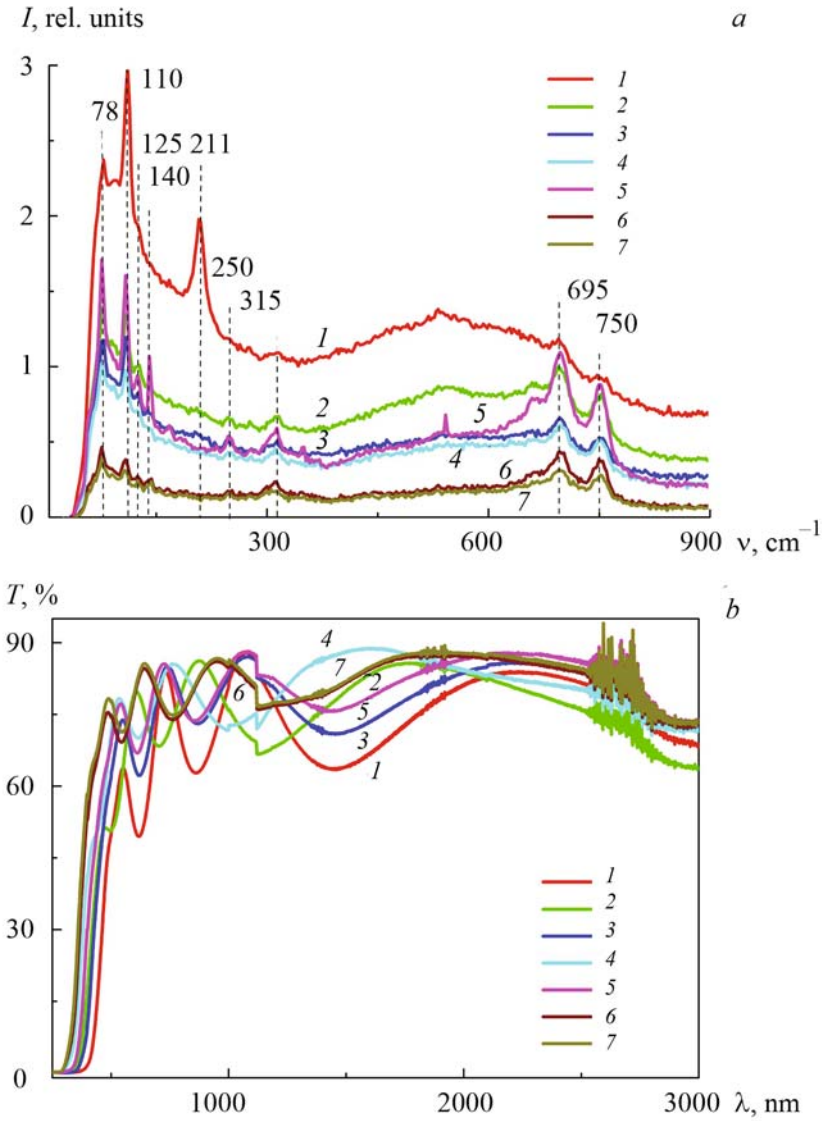

Fig. 2. Raman (a) and transmission spectra (b) of tin oxide films obtained by magnetron sputtering of a tin target with subsequent annealing in the air at 200°C for 2 h in the first stage and then at 325 (1), 350 (2), 375 (3), 400 (4), 425 (5), 450 (6), and 475°C (7) for 1 h in the second stage.

spectra are used to construct envelope curves $T_M(\lambda)$ and $T_m(\lambda)$ by interpolation of the transmission spectra between the experimental interference maxima and minima observed on them. Both linear interpolation and splines can be used to obtain envelope curves from the experimental data [30]. The dependence of the refraction index on the wavelength $n(\lambda)$ of the thin films studied was found using the following equations [30, 31]:

$$n(\lambda) = \left[\left(\frac{2n_s \left(T_M(\lambda) - T_m(\lambda)\right)}{T_M(\lambda) T_m(\lambda)} + \frac{n_s^2 + 1}{2} \right) + \sqrt{\left(\frac{2n_s \left(T_M(\lambda) - T_m(\lambda)\right)}{T_M(\lambda) T_m(\lambda)} + \frac{n_s^2 + 1}{2} \right)^2 - n_s^2} \right]^{1/2}, \quad (1)$$

where n_s is the refraction index of the substrate given by the following equation:

$$n_s = \frac{1}{T_s} + \sqrt{\frac{1}{T_s^2} - 1}, \quad (2)$$

TABLE 1. Optical Characteristics and Thickness of Tin Oxide Films Synthesized at Different Temperatures in the Second Annealing Stage

Temperature in the second annealing stage, °C	Refraction index (λ = 550 nm)	Tauc optical gap, eV	Film thickness, nm
325	2.6	2.62	340
350	2.2	2.81	330
375	2.9	2.85	400
400	2.5	2.91	300
425	2.16	2.85	480
450	2	3.37	500
475	2	3.46	500

where T_s is the transmission coefficient of the substrate. For the glass substrates used $T_s = 0.9$. Using Eq. (2), we obtained $n_s = 1.595$. The results for our calculation of the refraction index are given in Fig. 3. It is seen that the refraction index dependence on λ is nonmonotonic. A similar nature of the curves $n_s(\lambda)$ in the visible spectral region for SnO_2 films has already been noted by Kondrashin [30].

The films thickness was determined using the formula of Kondrashin [30]:

$$d = \frac{A\lambda_1\lambda_2}{2\left[n(\lambda_1)\lambda_2 - n(\lambda_2)\lambda_1\right]}, \tag{3}$$

where λ_1 and λ_2 are the wavelengths corresponding to adjacent extreme points in the transmission spectrum, while $A = 1$ for two adjacent extrema of the same type (max–max and min–min), and $A = 0.5$ for two adjacent extrema of opposite types (max–min and min–max). These results are presented in Table 1. The range of values found for the thickness d of the tin oxide films prepared with different temperatures of the second annealing stage evaluated using Eq. (3) was 340–500 nm. The discrepancies in the values of d largely arise because there is quite a large scatter of the film thickness in the radial direction in the case of magnetron sputtering. The samples cut from segments of the substrate located near its center have greater thickness.

In order to determine the absorption edge (Tauc optical gap) of the tin oxide films, the measured transmission spectra were recalculated to give absorption spectra using the following equation [32]:

$$\alpha(\lambda) = \frac{1}{d}\ln\left[\frac{\left(n(\lambda)-1\right)\left(n(\lambda)-n_s\right)\left[\left(\frac{T_M(\lambda)}{T_m(\lambda)}\right)^{1/2}+1\right]}{\left(n(\lambda)+1\right)\left(n(\lambda)+n_s\right)\left[\left(\frac{T_M(\lambda)}{T_m(\lambda)}\right)^{1/2}-1\right]}\right]. \tag{4}$$

The width of the band gap of both direct-bandgap and indirect-bandgap semiconductors can be found from the dependence of their absorption coefficient α on the radiation energy $h\nu$ plotted in coordinates $(\alpha h\nu)^2$ versus $h\nu$ or $(\alpha h\nu)^{1/2}$ versus $h\nu$ [33, 34], Figure 4 shows the absorption spectra in coordinates $(\alpha h\nu)^2$ versus $h\nu$ for films prepared at different temperatures in the second annealing stage.

The Tauc optical gap was determined from the linear approximation of the dependence of the absorption coefficient on the electromagnetic radiation frequency in coordinates $(\alpha h\nu)^2$ versus $h\nu$ indicating the existence of direct optical transitions (Table 1). Analysis of the structural features of the samples indicated that they contain SnO, SnO_2 as well as nonstoichiometric phases, which suggests the existence of both direct and indirect optical transitions. However, due to strong disorder of the tin oxide film structure and the existence of deep tails in the density of states in the band gap of

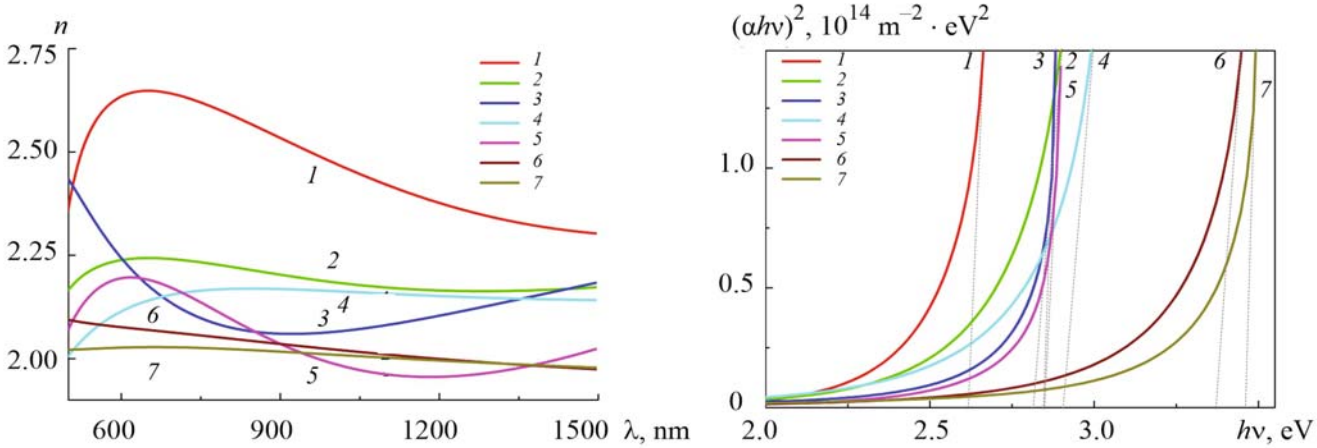

Fig. 3. Dependence of the refraction index on the wavelength for tin oxide films prepared by magnetron sputtering of a tin target with subsequent annealing in the air at 200°C for 2 h in the first stage and at 325 (1), 350 (2), 375 (3), 400 (4), 425 (5), 450 (6), and 475° (7) for 1 h in the second stage.

Fig. 4. Absorption spectra in coordinates $(\alpha h\nu)^2$ vs. $h\nu$ of tin oxide films obtained by magnetron sputtering of a tin target with subsequent annealing in the air at 200°C for 2 h in the first stage and at 325 (1), 350 (2), 375 (3), 400 (4), 425 (5), 450 (6), and 475°C (7) for 1 h in the second stage.

optical Tauc gap energies (corresponding to the optical width of the band gap of the films studied), the curves for $\alpha(\nu)$ determined from the linear approximation plotted in coordinates $(\alpha h\nu)^{1/2}$ versus $h\nu$ and $(\alpha h\nu)^2$ versus $h\nu$ differ only slightly for samples obtained at the same temperature in the second annealing stage. Table 1 shows that a tendency arises with higher temperature in the second annealing stage for expansion of the optical Tauc gap, which varies in the range 2.62–3.46 eV. This effect of second-stage annealing at higher temperatures is related to more complete oxidation of SnO and a greater amount of the SnO_2 phase in the films. This conclusion is in good accord with the structural data results for the tin oxide films by x-ray diffraction and Raman spectroscopy. Varying the annealing temperature permits us to obtain materials with an altered Tauc optical gap width, which can be useful for the creation of light filters.

Conclusions. Feasibility was shown for changing the crystal structure, phase composition, and optical characteristics of thin tin oxide films obtained by magnetron sputtering on glass substrates with subsequent two-stage annealing in the air in the temperature range 325–475°C in the second stage. The x-ray diffraction, Raman spectral, and transmission spectroscopy results for the structural and optical properties of the films in the UV and visible regions indicate the following conclusions.

Magnetron sputtering of tin films on glass substrates and subsequent oxidative annealing was found to yield thin polycrystalline disordered tin oxide films, in which SnO, Sn_2O_3, and Sn_3O_4 are present in addition to the SnO_2 phase. The composition of the tin oxide films can be controlled by changing the temperature of the second annealing stage. Raising this temperature leads to a greater content of the SnO_2 phase in the films. Variation of the second stage annealing temperature permits us to obtain tin oxide films with a high transmission coefficient (up to ~82%) in the visible spectral region as well as to alter the optical properties of the films (the transmission index in the range 2–2.6 and the Tauc optical gap in the range 2.62–3.46 eV).

Acknowledgments. The authors express their gratitude to S. V. Zlotskii and V. I. Shimanskii for carrying out the x-ray structural measurements of the samples and to O. V. Korolik for taking the Raman spectra of the films.

This work was carried out in the framework of the Materials Science, New Materials and Technology Project of the Belarusian Foundation for Fundamental Research No. F22UZB-056 State Scientific Programs Project 2.14 (NIR 3) and was supported by the International Cooperation Research Fund under the aegis of the Joint Institute and Innovation Center of the Belarusian State University (Dalian, China) and Belarusian State University (Minsk, Belarus) (Grant No. ICR2202).

REFERENCES

1. M. Z. Iqbal, F. Wang, R. Hussain, M. Y. Rafique, S. Ali, and I. Ali, *Mater. Focus*, **3**, 1–6 (2014).
2. Y. Li, T. Cui, L. Zhang, Y. M. Ma, and G. T. Zou, *J. Phys.: Cond. Matter*, **19**, No. 32, 425230(1–10) (2007).
3. M. Ristić, M. Ivanda, S. Popović, and S. Musić, *J. Non-Crystall. Solids*, **303**, No. 2, 270–280 (2002).
4. C. Li, M. Zhang, X. H. Wang, L. Yao, L. Ma, and W. Shen, *Nanoscale Res. Lett.*, **6**, No. 1, 615(1–7) (2011).
5. V. Ksenevich, V. Dorosinets, D. Adamchuk, J. Macutkevic, and J. Banys, *Materials*, **13**, No. 23, 5415 (1–14) (2020).
6. M. Tatzill and U. Diebold, *Prog. Surface Sci.*, **79**, 47–154 (2005).
7. O. L. Bersirova, L. I. Bruk, A. I. Dikusar, M. I. Karaman, S. P. Sidel'nikova, A. V. Simashkevich, D. A. Sherban, and Yu. S. Yapontseva, *Surface Eng. Appl. Electrochem.*, **43**, No. 6, 443–452 (2007).
8. V. F. Gromov, G. N. Gerasimov, T. V. Belysheva, and L. I. Trakhtenberg, *Russ. Chem. J.*, **52**, No. 5, 80–87 (2008).
9. K. P. Bogdanov, D. Ts. Dimitrov, O. F. Lutskaya, and Yu. M. Tairov, *Semiconductors*, **32**, No. 10, 1033–1035 (1998).
10. B. Yuliarto, G. Gumilar, and N. L. W. Septiani, *Adv. Mater. Sci. Eng.*, No. 12, Article ID 694823(1–14) (2015).
11. T. Oshima, T. Okuno, and S. Fujita, *Jpn. J. Appl. Phys.*, **48**, Article ID 120207(1–3) (2009).
12. M. Alaf, D. Gultekin, and H. Akbulut, *Acta Phys. Polonica A*, **123**, No. 2, 323–325 (2013).
13. Y. C. Lu, C. Ma, T. Alvarado, T. Kidera, N. Dimov, Y. S. Meng, and S. Okada, *J. Power Sources*, **284**, 287–295 (2015).
14. V. K. Ksenevich, D. V. Adamchuk, V. B. Odzhaev, and P. Zhukowski, *Acta Phys. Pol. A*, **128**, No. 5, 861–863 (2015).
15. D. V. Adamchuck and V. K. Ksenevich, *Prib. Metody Izmer.*, **10**, No. 2, 138–150 (2019).
16. D. V. Adamchuck, V. K. Ksenevich, N. A. Poklonskii, M. Navickas, and J. Banys, *Lith. J. Phys.*, **59**, No. 4, 179–187 (2014).
17. D. V. Adamchuck, V. K. Ksenevich, N. A. Poklonski, and A. I. Kavaleu, *Izv. Nats. Akad. Navuk Belarusi*, *Ser. Fiz.-Mat. Nauk*, **56**, No. 1, 102–113 (2020); doi: 10.29235/1561-2430-2020-56-1-102-113.
18. E. M. F. Vieira, J. P. B. Silva, K. Veltruski, V. Matolin, A. L. Pires, A. M. Pereira, M. J. M. Gomes, and L. M. Goncalves, *Nanotechnology*, **30**, No. 43, Article ID 435502(1–22) (2019).
19. A. Shanmugasundaram, P. Basak, L. Satyanarayana, and S. V. Manorama, *Sens. Actuators B Chem.*, **185**, 265–273 (2013).
20. L. Li, C. Zhang, and W. Chen, *Nanoscale*, **7**, No. 28, 12133–12142 (2015).
21. W. Zeng, Y. Liu, G. Chen, H. Zhan, J. Mei, N. Luo, Z. He, and C. Tang, *RSC Adv.*, **10**, No. 50, 29843–29854 (2020).
22. M. Saravanakumar, S. Agilan, N. Muthukumarasamy, and V. Rukkumani, *Int. J. Chem. Sci.*, **13**, No. 2, 605–612 (2015).
23. P. Boroojerdian, *Int. J. Nanosci. Nanotechnol.*, **9**, No. 2, 95–100 (2013).
24. L. Sangaletti, L. E. Depero, B. Allieri, F. Pioselli, E. Comini, G. Sberveglieri, and M. Zocchi, *J. Mater. Res.*, **13**, No. 9, 2457–2460 (1998).
25. M. Khosravi-Nouri, N. Shahtahmassebi, E. Attaran-Kakhki, and G. Zohuri, *Mater. Phys. Mech.*, **17**, 29–32 (2013).
26. Y. Q. Guo, R. Q. Tan, X. Li, J. H. Zhao, Z. L. Luo, C. Gao, and W. J. Song, *Cryst. Eng. Commun.*, **13**, 5677–5680 (2011).
27. B. Eifert, M. Becker, C. T. Reindt, M. Giar, L. Zheng, A. Polity, Y. He, C. Heiliger, and P. J. Klar, *Phys. Rev. Mater.*, **1**, No. 1, Article ID 014602(1–6) (2017).
28. C. Guillén and J. Herrero, *J, Mater. Sci. Tech.*, **35**, No. 8, 1706–1711 (2019).
29. D. Tuschel, *Spectroscopy*, **33**, No. 12, 12–19 (2018).
30. V. I. Kondrashin, *Tekh. Nauki. Élektronika, Izmerit. Radiotekh.*, **2**, No. 38, 93–101 (2016).
31. V. V. Brus, Z. D. Kovalyuk, and P. D Maryanchuk, *Tech. Phys.*, **57**, 1148–1151 (2012).
32. V. V. Brus, M. N. Solovan, E. V. Maistruk, I. P. Kozyarskii, P. D. Maryanchuck, K. S. Ulyanytsky, and J. Rappich, *Phys. Solid State*, **56**, 1947–1951 (2014).
33. D. L. Wood and J. Tauc, *Phys. Rev. B*, **5**, 3144–3151 (1972).
34. J. Klein, L. Kampermann, B. Mockenhaupt, M. Behrens, J. Strunk, and G. Bacher, *Adv. Func. Mater.*, **33**, Article ID 2304523(1–19) (2023).